Journal of Materials Chemistry B

ROYAL SOCIETY OF CHEMISTRY

PAPER

View Article Online
View Journal

Cite this: DOI: 10.1039/d0tb00137f

Nanosized copper(II) oxide/silica for catalytic generation of nitric oxide from *S*-nitrosothiols

Kostiantyn Kulyk,[a] Liana Azizova,[ab] James M. Cunningham,[b] Lyuba Mikhalovska,[b] Mykola Borysenko[a] and Sergey Mikhalovsky *[ac]

Nitric oxide NO, mediates inflammatory and thrombotic processes and designing biomaterials capable of releasing NO in contact with biological tissues is considered to be a major factor aimed at improving their bio- and haemocompatibility and antibacterial properties. Their NO-releasing capacity however is limited by the amount of the NO-containing substance incorporated in the bulk or immobilised on the surface of a biomaterial. An alternative approach is based on the design of a material generating nitric oxide from endogenous NO bearing metabolites by their catalytic decomposition. It offers, at least in theory, an unlimited source of NO for as long as the material remains in contact with blood and the catalyst maintains its activity. In this paper we studied the catalytic properties of novel nanostructured CuO/SiO_2 catalysts in generating NO by decomposition of *S*-nitrosoglutathione (GSNO) *in vitro*. CuO/SiO_2 catalysts with different CuO loadings were synthesized by chemisorption of copper(II) acetylacetonate on fumed nanosilica followed by calcination. CuO content was controlled by a number of chemisorption–calcination cycles. Fourier-transform infrared spectroscopy and thermogravimetric analysis confirmed the formation of CuO/SiO_2 nanoparticles (NPs) with particle size of CuO phase in the range from 71 to 88 nm. Scanning electron microscopy images revealed a uniform distribution of NPs without their sintering or agglomeration. All the materials of the CuO/SiO_2 NP series exhibited NO-generating activity from GSNO confirmed by the Griess assay and by measuring the concentration of nitrite and nitrate anions in model solutions such as phosphate buffered saline and bovine serum. This activity is dependent on the material specific surface area and CuO exposure on the surface rather than CuO bulk content. The rate of NO production increased at higher initial concentration of the NO-bearing substrate studied in the range between 0.01 mM and 1.0 mM RSNO, which covers its physiological level. CuO/SiO_2 NPs can be used to design polymers with NO generating properties at blood-biomaterial interface which are expected to have improved biocompatibility thus enhancing their potential for medical applications such as surgical tubing, peripheral venous catheters, auxiliary blood circulation devices and drug-eluting balloons.

Received 14th January 2020,
Accepted 6th April 2020

DOI: 10.1039/d0tb00137f

rsc.li/materials-b

Introduction

At present, biomedical implantable devices have an enormous impact on public health and quality of life. The global market for biomaterials was estimated at over €4 billion in the late 1980s, and has been projected to reach $207 billion by 2024 from $105 billion in 2019.[1,2] The rising demand to incorporate artificial devices into the human body is explained by the increased proportion of elderly in the worldwide population and by the sequential growth in age-related physical disabilities.[3] Blood-contacting implants such as vascular grafts, intravascular catheters, coronary artery and vascular stents constitute a major fraction of the clinically used biomaterials.[2] Thrombogenesis is the most common and severe problem, associated with the use of such implants, as it can cause functional failures and lethal outcomes;[4–9] therefore substantial efforts are aimed at developing novel antithrombotic biomaterials. It is well-established that nitric oxide (NO), a signalling molecule continuously released by endothelial cells *in vivo*, is an effective inhibitor of platelet adhesion and can prevent thrombus formation and promotes endothelialization.[4,7,10,11] The role of NO fluxes in maintaining thromboresistance of endothelial cell walls has been recognized in the early 1990s. This discovery encouraged numerous studies directed at improving the biocompatibility of materials *via* incorporation of NO-releasing compounds into biomaterial coatings. Advances of this therapeutic strategy have been

[a] Chuiko Institute of Surface Chemistry, 17 General Naumov Street, 03164 Kyiv, Ukraine. E-mail: sergeymikhalovsky@gmail.com
[b] University of Brighton, School of Pharmacy and Biomolecular Sciences, BN2 4GJ, Brighton, UK
[c] ANAMAD Ltd, Sussex Innovation Centre, Science Park Square, Falmer, Brighton, BN1 9SB, UK

comprehensively summarized in a number of recent reviews.[12–17] Despite its proven efficiency, the NO-releasing coating approach has an unsolvable limitation set by the finite reservoir of the NO donor compound that can be loaded within a coating. In response to a compelling need for alternative approaches, a lot of effort has recently been focused on the design of coatings that mimic endothelium function by continuous generation of NO from endogenous blood components called *S*-nitrosothiols (RSNO). Human plasma contains 7×10^{-6} M *S*-nitrosothiols, including *S*-nitrosoalbumin and *S*-nitrosoglutathione, which could potentially be used as an unlimited precursor source of NO circulating *in vivo*.[4,18] The natural endothelium-derived NO flux is in the range from 0.5×10^{-10} to 4×10^{-10} mol cm^{-2} min^{-1}, while NO surface flux of 3×10^{-8} mol cm^{-2} min^{-1} was reported to inhibit platelet adhesion by as much as 87%.[19] The results obtained by several research groups clearly demonstrated a strong potential of the *in situ* NO-generating approach to enhance the biocompatibility of biomaterials. Multiple studies have shown that NO generation from physiological concentrations of RSNOs could be effectively catalyzed by immobilized copper compounds such as Cu(II) complexes,[20–28] copper-containing metal–organic frameworks (MOFs)[29–32] and copper-polydopamine complexes.[24,25,33] Apart from complex compounds, successful use of metallic copper-doped TiO_2 films and polymer coatings containing nano-copper for NO generation has also been reported.[34–36] However, so far designing catalytic surface that can actively generate NO has faced a number of limitations such as complicated synthesis and modification steps, the difficulties in catalyst content control and catalyst toxicity.

The transition from conventional to nanosized materials represents a promising direction for improving the activity, selectivity and stability of heterogeneous catalysts.[37,38] The use of an inorganic support material such as nanosilica can not only stabilize the nanoparticle dispersion and thereby the catalytic efficiency of the active phase, but also securely immobilize the active component while maintaining its functional availability. The design of RSNO-modified silica particles by grafting the silica surface with *S*-nitroso-*N*-acetylpenicillamine, *S*-nitroso-*N*-acetylcysteine, or *S*-nitrosocysteine has been reported.[39,40]

Among other materials, silica is the most widely used scaffold and reinforcing filler in different polymers enabling the design of different NO generating polymers. The versatility of CuO/SiO_2 nanocomposite synthesis allows fine tuning of its catalytic properties and thus control of NO flux generation and its therapeutic effectiveness. The aim of our research has been to synthesize and characterize a novel nanosized catalyst CuO/SiO_2 capable of generating NO by decomposition of RSNO under physiological conditions.

Materials and methods

Chemicals

Fumed silica A-300 with specific surface area of 385 m^2 g^{-1} and primary particle size of ~8 nm in diameter was supplied by a pilot plant of the Chuiko Institute of Surface Chemistry in Kalush, Ukraine. Copper oxide precursor – copper(II) acetylacetonate, $Cu(acac)_2$ was purchased from Acros Organics, UK. *S*-Nitrosoglutathione (GSNO), Griess reagent (G4410), sodium nitrite ($NaNO_2$), sodium nitrate ($NaNO_3$), phosphate buffered saline (PBS) and adult bovine serum were purchased from Sigma, UK.

Preparation of CuO/SiO_2 nanosized compositions

The nanosized CuO/SiO_2 was synthesized by a liquid phase method. First, fumed silica was modified by $Cu(acac)_2$ chemisorption. To achieve completeness of the chemisorption reaction, a 1 : 1 molar ratio of $\equiv$Si–OH (surface silanol groups) to $Cu(acac)_2$ was used. The reaction was carried out in anhydrous carbon tetrachloride (CCl_4). $Cu(acac)_2$ (0.13 g) was placed in a two-neck round-bottom flask with a mechanical stirrer and dissolved in CCl_4 (50 mL) at 76 °C. Fumed silica (1 g) hitherto calcinated for 1 h at 500 °C was slowly added into the reactor. The suspension was boiled with a reflux condenser for 1 h. Silica thus modified by grafted copper acetylacetonate groups was separated from the reaction mixture by filtration. During filtration the recovered material was repeatedly washed with CCl_4 in order to remove unreacted $Cu(acac)_2$. Then, the filtered material was dried at room temperature for 24 h. Finally, the modified silica was calcinated at 550 °C to obtain CuO/SiO_2 nanocomposite. The chemisorption and oxidative calcination stages of synthesis were repeated up to four times in order to obtain nanocomposites with different loadings of copper oxide nanoparticles. The samples were coded CuO/SiO_2_*X*, where *X* (from 1 to 4) indicated the number of reiterations of chemisorption–calcination cycles.

Characterization of CuO/SiO_2 nano-oxides

Infrared spectroscopy (IR). IR spectroscopy measurements were performed using a Thermo Nicolet Nexus Fourier-transform infrared spectrometer in the 400–4000 cm^{-1} range, working in "Nexus Smart Collector" mode and averaging 50 scans with a resolution of 4 cm^{-1}.

Powder X-ray diffraction (XRD). The powder XRD patterns were registered using an automatic diffractometer DRON-3M with copper anode-induced radiation and nickel filter (Burevestnik, Russia). The measurements were performed in the mode of reflected rays and the Bragg–Brentano geometry of focusing. XRD scans were collected in the 10–70° 2θ range. The average size of CuO nanocrystallites produced was determined according to the Scherrer equation.

Low temperature nitrogen adsorption analysis. Nitrogen adsorption–desorption measurements were performed using a gas adsorption analyzer Autosorb-1 (Quantachrome Instruments, UK). Prior to the low temperature nitrogen adsorption at 77.3 K all the nano-oxide samples were outgassed at 200 °C for 3 h. The results were analyzed using ASiQwin software from Quantachrome. The specific surface area values were calculated using the Brunauer–Emmett–Teller (BET) equation.

Thermogravimetric analysis (TGA). Thermal analysis (TG/DTG/DTA) of $Cu(acac)_2$ chemisorbed on silica samples was carried out in air at 20–1000 °C using a Derivatograph

Q-1500D (Paulik, Paulik & Erdey, MOM, Budapest) at a heating rate of 10 °C min^{-1}.

Quantitative analysis of copper in CuO/SiO_2 nano-oxides. The amount of copper oxide in each sample was measured using a PerkinElmer Optima 2100 DV Inductively Coupled Plasma Optical Emission Spectrometer (ICP-OES). For analysis, 10 mg of each sample was mixed with 5 mL of 70% HNO_3 and heated for 10 min at 100 °C. After cooling, a precipitate of each sample was separated by elutriation and repetitively treated with 70% HNO_3 solution for 10 min at 100 °C. Then the mixture of the above solutions was diluted to 100 mL with de-ionized water and analyzed by ICP-OES. The calibration curve was constructed by using a copper standard calibration solution (PerkinElmer Pure, Quality Control Standard) and used to determine the concentration of the unknown analyte solutions. All measurements were performed in triplicate.

Scanning electron microscopy (SEM) and energy dispersive X-ray spectroscopy (EDS). The powders of CuO/SiO_2_1–4 preparations were placed on the adhesive carbon pads glued to stubs and the excess of powder was shaken off from the surface. Samples coated with platinum were then analyzed using a Zeiss Sigma Field Emission SEM (Zeiss, Germany). Elemental analysis was performed using Energy Dispersive X-ray Spectroscopy (EDS, Oxford Instruments, UK) linked to the SEM instrument. 10 kV voltage was used in EDS analysis and five fields over each sample surface were analyzed.

Nitric oxide measurement using Griess assay. The principal spontaneous oxidation product of NO in aqueous solution is nitrite (NO_2^-) while both nitrite and nitrate (NO_3^-) are produced in biological fluids such as blood plasma and serum.[41,42] The Griess assay is widely used to measure NO generation in *in vitro* conditions, including PBS and blood plasma. The assay may not measure the exact amount of NO but the measurements are proportional to NO concentration in the medium.[43,44]

Nitrite anions form a colored azo dye compound with the Griess reagent and its concentration was measured spectrophotometrically at 540 nm. Standard solutions of $NaNO_2$ in PBS at concentrations of 3–100 μM were prepared for plotting the standard curve. 100 μL samples of $NaNO_2$ standard solutions were placed into a 96-well plate followed by adding 100 μL of Griess reagent. Plates were incubated for 5–15 min and the absorbance measured using a Microplate Reader BioTek FLx800 (BioTek Instruments, USA). The catalytic activity of CuO/SiO_2 in NO generation was determined by incubation of 1 mg of solid catalyst with 0.5 mL of GSNO in PBS solution in the concentration range 0.01–1 mM for 30 min. For the time-dependent assay, tubes were incubated at 37 °C for 5–90 min.

To compare the catalytic activity of different catalyst preparations, 1 mg of each sample CuO/SiO_2_1–4 was incubated with 0.5 mL of 0.1 mM GSNO for 30 min. To study the dependence of NO release on the amount of copper, the amount of CuO/SiO_2_1 sample matching Cu^{2+} amount in the other three preparations (CuO/SiO_2_2–4 preparations with Cu^{2+} content 1.8 mg, 2.7 mg and 2.9 mg respectively) was used.

Measurement of nitrite and nitrate using an ion-selective electrode method. As an alternative to the Griess method for NO detection, ion-selective microelectrodes for independent measurement of both nitrite and nitrate ions was applied using an Arrowstraight™ Nitric Oxide (NO_2^-/NO_3^-) system, (Lazar Research Laboratories, Los Angeles, CA, USA). Freshly prepared 500 μM GSNO solution in PBS was used as a stock solution and its concentration was verified spectrophotometrically by measuring the UV absorption of the SNO group at 335 nm using the extinction coefficient of 922 M^{-1} cm^{-1}. Catalytic NO generation by powder compositions was performed in PBS and in bovine plasma. For that 1 mg of CuO/SiO_2 powder was incubated with 1 mL of 100 μM GSNO and 100 μM GSH in PBS or bovine serum at 37 °C for 1 h with gentle mixing in an orbital shaker. Glutathione (GSH) as a reducing agent was added because it is present at high concentration in blood but not in plasma.[45,46] After incubation, samples were spun down using filters with 10 kDa molecular weight cut-off (Amicon Centrifugal Filters, Merck) according to manufacturer's instructions the for measuring NO release in biological fluids. 200 μL of filtrate from each tube was injected in the system to measure NO_2^- and NO_3^- concentration. The quantification of NO release by the catalytic decomposition of GSNO was calculated by summation of the concentrations of NO_2^- and NO_3^- in each sample. As standards, serial dilutions of 0.1 M sodium nitrite and 0.1 M sodium nitrate solutions were used. Validation of NO amount in the samples was performed according to the manufacturer's manual using the software provided. All measurements were performed in triplicate. During NO measurements all solutions containing GSNO were shielded from light by wrapping with foil to prevent light triggered decomposition of GSNO.

Results and discussion

Four preparations of nanosized CuO/SiO_2 catalyst (CuO/SiO_2_1–4) with different loadings of CuO nanoparticles were produced using copper(II) acetylacetonate and fumed nanosilica as precursors. The applied synthetic procedure included a stepwise increment of the active CuO nanophase content in the sample. This was done by performing one to four reiteration cycles of $Cu(acac)_2$ chemisorption onto the surface of the support material and its subsequent thermal decomposition. Such a step-by-step functionalization protocol was used to increase the content of the active CuO nanoparticles while preventing their agglomeration. FTIR spectroscopy was used to study the structure of surface complexes in all the samples containing chemisorbed $Cu(acac)_2$. This method was also used to confirm the removal of organics after thermal decomposition of grafted groups and rehydroxylation of surface silanols. The thermal degradation profile of the samples modified with $Cu(acac)_2$, the thermal stability of grafted groups and the weight loss were studied by TGA. After oxidative calcination, the crystalline structure and nanoparticle size of the CuO/SiO_2_1–4 compositions were investigated by XRD. The surface morphology and preliminary Cu content were examined by SEM/EDS. Quantitative chemical analysis was performed with ICP-OES. The specific surface area was measured by low-temperature N_2 adsorption analysis. After characterization,

all synthesized catalysts CuO/SiO_2_1–4 were tested for their ability to generate NO from GSNO in physiological media.

Synthesis and characterization of nanosized CuO/SiO_2 catalysts

Nanosilica was selected to be the carrier for the catalytic nanoparticles of copper oxide to stabilize their dispersion and improve the oxygen exchange rate, which is required for high catalytic performance. SiO_2 is a biocompatible inorganic carrier possessing a high specific surface area combined with excellent chemical and thermal stability.[47] An additional advantage of nanosilica is that its surface functional groups can be controllably functionalized with organometallic precursors of catalytic oxide nanoparticles. The first stage of synthesis was the surface modification of the support material.

When pretreated, surface silanol groups of nanosilica become highly reactive and can be functionalized *via* electrophilic substitution of the silanol proton.[48] Thus, under conditions of synthesis applied in the present work, interaction of copper(II) acetylacetonate with the silanol groups of the silica surface led to the formation of grafted groups ≡SiOCu(acac) and release of acetylacetone in 1:1:1 ratio as shown in Scheme 1.

The chemical interaction of metal acetylacetonates and the silica surface is accompanied by their physical adsorption; the unreacted $Cu(acac)_2$ and acetylacetone released upon chemisorption were removed from silica by vigorous washing with warm CCl_4 during its filtration.

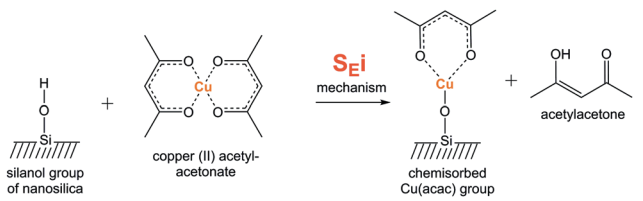

Scheme 1 Chemisorption of $Cu(acac)_2$ on the surface of fumed silica.

It is crucial for the synthesis to remove all non-chemisorbed modifier from the surface of the nanosilica leaving only the chemisorbed groups for further oxidation The number of silanol groups per unit of surface area, when the surface is fully hydroxylated, is considered to be constant.[49] This constant, $\alpha OH_{average}$, has a numerical value of 4.6 OH-groups per nm^2 and is known in the literature as Zhuravlev constant.[49] Selective adsorption or chemisorption occurs primarily on isolated singular silanol groups. A sufficient distance between those groups helps preventing agglomeration of CuO particles formed from chemisorbed $Cu(acac)_2$ during the stage of thermal oxidation.

Infrared spectroscopy

Substitution for silanols and formation of grafted surface groups *via* the reaction described above (Scheme 1) was validated by FTIR spectroscopy. The most characteristic infrared vibrational frequency region for metal acetylacetonates lies between 1500 and 1600 cm^{-1}.[50,51] The strong absorption band at 1579 cm^{-1}, which is not found in the spectra of unmodified silica, corresponds to the stretching frequency of the C=O group of a pseudo aromatic copper(II) surface complex. Such a shift in carbonyl group absorption, which typically lies in the 1700 cm^{-1} region, proves the coordination of Cu^{2+} ions through the enol tautomer of the acetylacetonate ligand. The band at 1528 cm^{-1} is assigned to a perturbed C=C bond of the surface complex. These IR absorption bands were distinguishable for all samples with chemisorbed $Cu(acac)_2$ (Fig. 1A).

After oxidative calcination at 550 °C in air the organic part of the synthesized materials was burned off and vibrational bands assigned to chemisorbed $Cu(acac)_2$ disappeared (Fig. 1B).

To further confirm the formation of chemisorbed surface complexes, the IR absorption in the 3750 cm^{-1} region has been examined. The characteristic stretching frequency for the silanol group O–H is exactly 3750 cm^{-1}. Usually O–H stretch is a strong band in the spectra of highly dispersed silica. In the

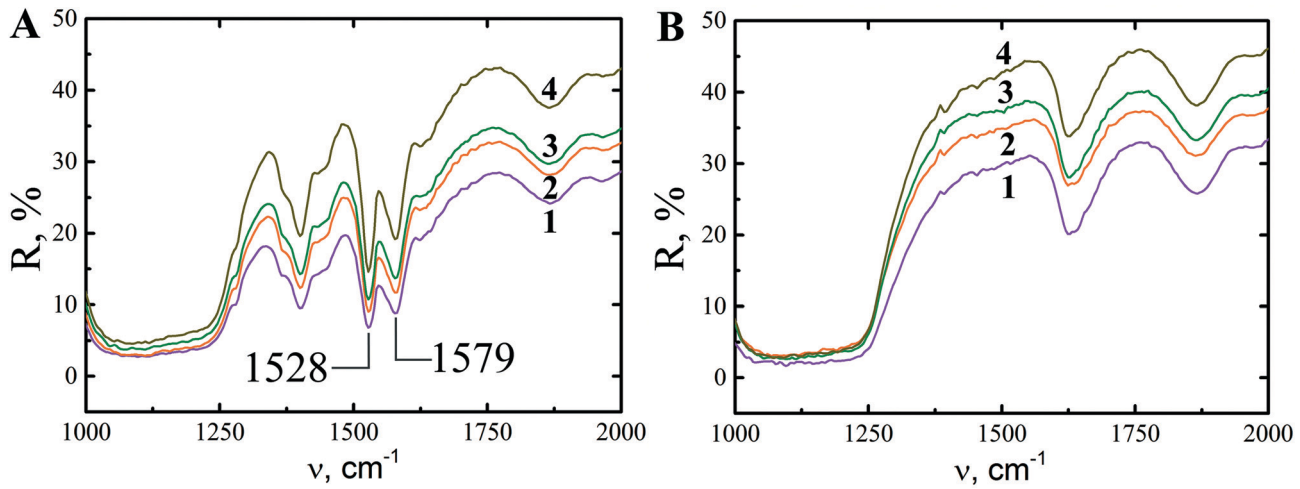

Fig. 1 FTIR spectra of samples CuO/SiO_2_1 (1), CuO/SiO_2_2 (2), CuO/SiO_2_3 (3) and CuO/SiO_2_4 (4) modified with $Cu(acac)_2$ in the silanol group adsorption region. Measurements were performed before (A) and after (B) oxidative calcination at 550 °C.

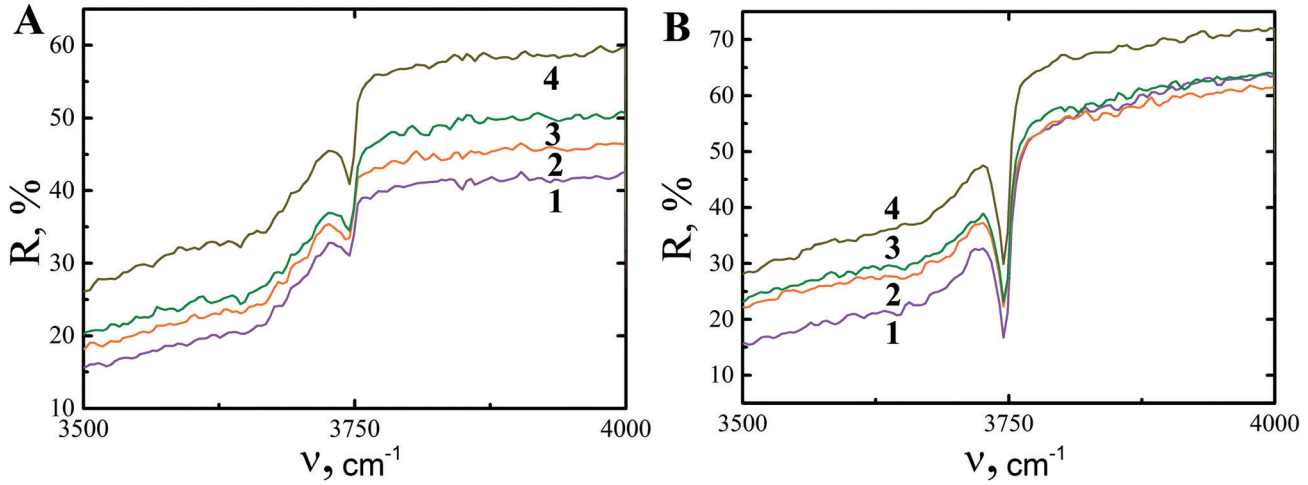

Fig. 2 FTIR spectra of samples CuO/SiO_2_1 (1), CuO/SiO_2_2 (2), CuO/SiO_2_3 (3) and CuO/SiO_2_4 (4) modified with $Cu(acac)_2$. Measurements were performed before (A) and after (B) oxidative calcination at 550 °C.

samples modified with $Cu(acac)_2$ this vibrational band was significantly lowered due to chemisorption of $Cu(acac)_2$ (Fig. 2A).

After oxidative calcination the intensity of the silanol O–H stretching absorption band was restored due to elimination of the acetylacetonate ligand and subsequent rehydroxylation of the surface (Fig. 2B).

Thermogravimetric analysis

To investigate the thermal oxidative destruction of $Cu(acac)_2$ chemisorbed on oxide surfaces, and to determine the temperature range for calcination of nano-oxide precursor samples, TGA was performed (Fig. 3). The DTA profile demonstrates that thermal decomposition of grafted copper acetylacetonate groups in air is accompanied by exothermic effects in the region from 50 to 330 °C. The absence of endothermic effects indicates that no sublimation of $Cu(acac)_2$ was occurring in this temperature range, as sublimation is an endothermic process. It indicates the completeness of the chemisorption reaction and absence of physisorbed species which were apparently removed during the filtration stage. Exothermic effects observed in the temperature range 50–330 °C correspond to the oxidative destruction and desorption of acetylacetonate ligands of the chemisorbed $Cu(acac)_2$. This process leads to the formation of CuO nanoparticles uniformly distributed over a highly dispersed SiO_2 support (Scheme 2).

Fig. 3 also shows that TG/DTG curves concur within the temperature range of exothermic effects. The most intensive thermal decomposition of acetylacetonate ligands occurred between 100 and 350 °C. The small gradual weight loss that happened at temperatures from 350 and up to 1000 °C is associated with dehydroxylation of single silanols.[49,52]

The weight losses, Δm, for the samples were found to decrease with an increase in the copper content. Thus Δm for the samples CuO/SiO_2_1 was 9.1%; CuO/SiO_2_2 – 7.4%; CuO/SiO_2_3 – 7.4%; and CuO/SiO_2_4 – 5.7% (Fig. 3). These data are consistent with the postulated reaction mechanism as the Δm values indicate that only one acetylacetonate ligand is lost per one Cu^{2+} chemisorbed on the SiO_2 support (Scheme 2).

Based on TGA data it was expected that oxidation and desorption of organic ligands completes at around 350 °C for all studied samples. Because of this, the calcination of $Cu(acac)_2$-modified samples was carried out at a temperature of 550 °C. This temperature regime ensured that all organics were burned off and CuO/SiO_2 oxide nanoparticles were formed as shown in Scheme 2.

X-ray powder diffraction analysis

The powder XRD measurements evidenced the nanocrystalline nature of CuO in the CuO/SiO_2_1–4 preparations (Fig. 4). Sharp peaks registered in the diffractograms of the samples calcinated at 550 °C correspond to the monoclinic CuO (JCPDS # 80-1916) (peaks labelled CuO and * in Fig. 4).

The broadened shape of the CuO peaks distinctly indicated the nanocrystallinity. Full width at half maximum of the most intense line of CuO peaks was used for the calculation of particle sizes according to the Scherrer equation. The average crystallite sizes were determined to fall within the range of 71–88 nm (Table 1). The increase of the copper content in the sample, did not cause the agglomeration and growth of CuO crystallite size. Prevention of CuO nanoparticles agglomeration and preservation of their nanocrystallinity could be explained by the stabilizing effect of the silica support and by a stepwise increase of the active oxide phase concentration during synthesis. The diffraction lines corresponding to the CuO nanoparticles intensified with increase of the number of chemisorption–calcination cycles, indicating the increased CuO content in the sample (Fig. 4).

The N_2 BET surface areas of CuO/SiO_2_1–4 preparations are presented in Table 1. The initial silica sample (calcinated at 550 °C as the rest of the samples) exhibits a surface area of 385 $m^2 g^{-1}$. Successive reiterations of chemisorption–calcination stages of synthesis and sequential growth of CuO nanoparticle content led to a gradual decrease of the surface area, reaching

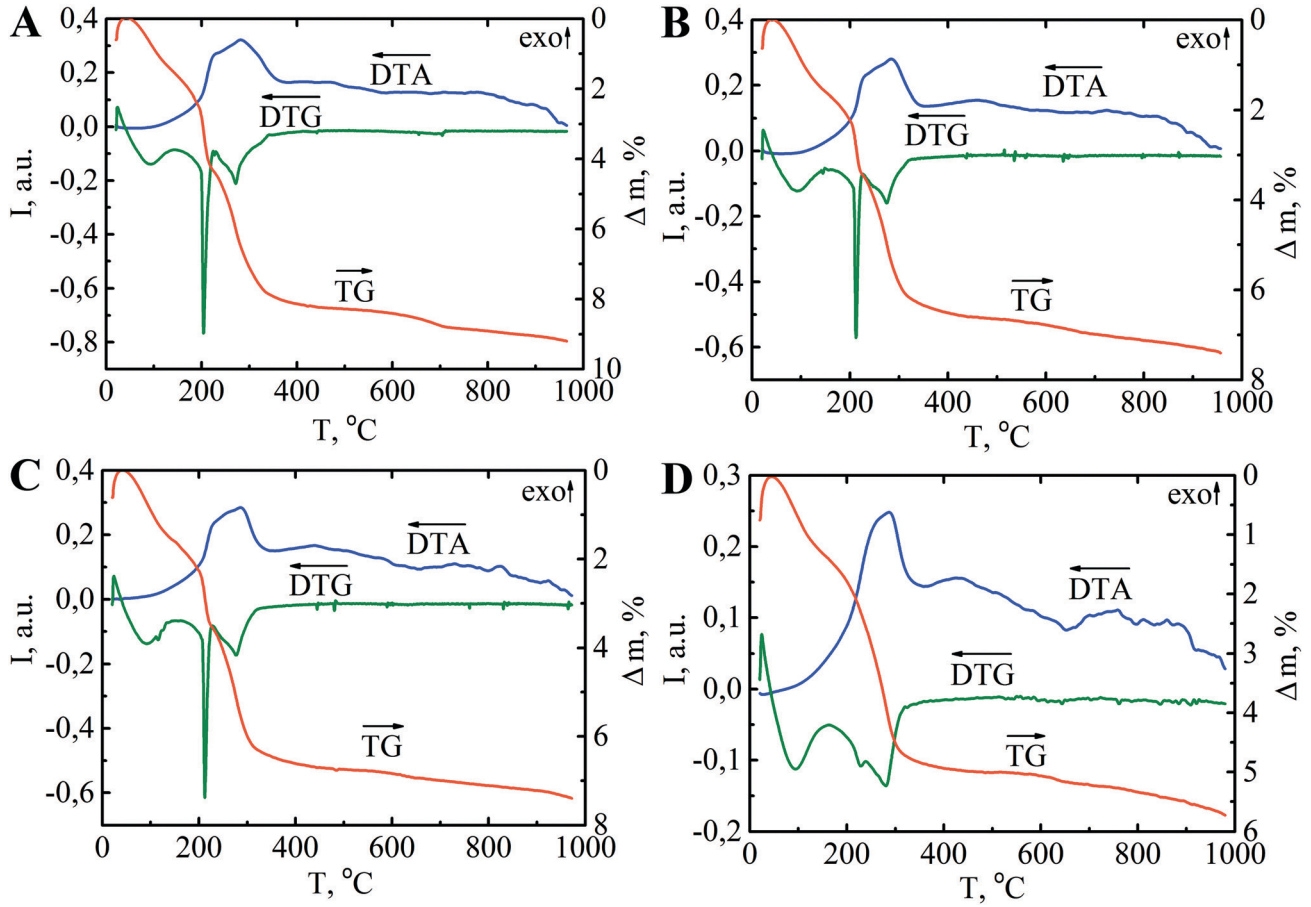

Fig. 3 TGA of non-calcinated samples: CuO/SiO_2_1 (A), CuO/SiO_2_2 (B), CuO/SiO_2_3 (C) and CuO/SiO_2_4 (D).

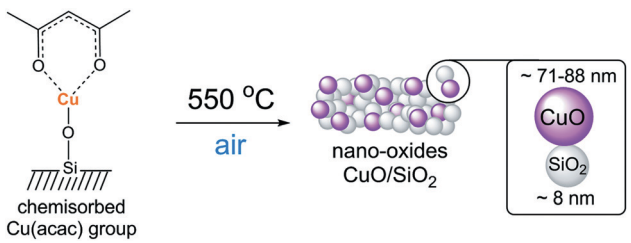

Scheme 2 Thermal decomposition of grafted copper(II) acetylacetonate groups leading to formation of nanosized CuO/SiO_2 composition.

325 $m^2\ g^{-1}$ for the CuO/SiO_2_4 preparation and revealing a loss of only ~16%. Maintaining such a high surface area even after four cycles of chemisorption–calcination is a notable synthetic result which confirms that nanosilica prevents sintering and agglomeration of nanocrystalline copper(II) oxide.

Scanning electron microscopy

The surface morphology of nanosized CuO/SiO_2 was studied with SEM. High resolution scanning electron micrographs of CuO/SiO_2_1 preparation showed the presence of particles in the range of 10–50 nm in diameter and larger size aggregates (Fig. 5). The small particles of 8–10 nm in diameter are most likely primary SiO_2 nanoparticles which formed aggregates with each other and formed also larger aggregates by interaction with CuO. This observation is in agreement with the conclusion that nanosilica enabled good dispersion of CuO nanoparticles and prevented their sintering, which is a major problem of all highly dispersed nanocatalysts prepared by treatment at high temperatures.

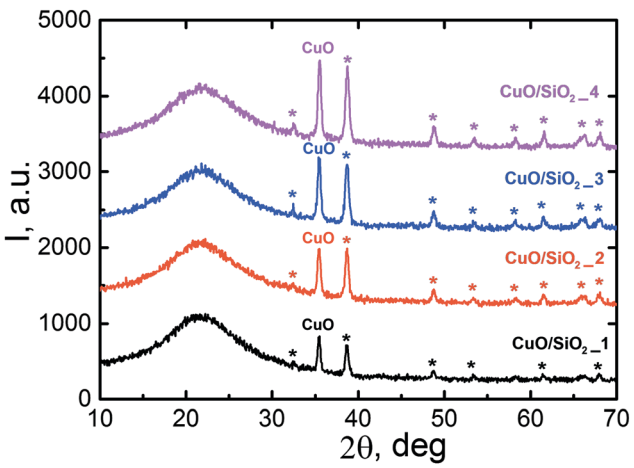

Fig. 4 Powder X-ray diffraction (XRD) analysis of nanosized CuO/SiO_2_1–4 compositions.

Table 1 Characteristics of nanosized CuO/SiO_2 compositions based on silica A-300

Preparation	CuO content (wt%)	BET SA ($m^2\ g^{-1}$)	Crystallite size of CuO (nm)
SiO_2	0	385	n/a[a]
CuO/SiO_2_1	2.6	382	88
CuO/SiO_2_2	4.8	324	79
CuO/SiO_2_3	7.1	320	85
CuO/SiO_2_4	7.6	325	71

[a] Not applicable.

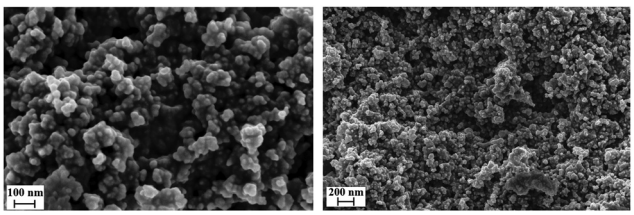

Fig. 5 SEM images of nanosized CuO/SiO_2_1.

The presence of copper on each nanocatalyst surface was assessed by energy-dispersive X-ray spectroscopy. The average amount of copper detected in each preparation (not shown) was in agreement with the data obtained by ICP-OES analysis described above. However, the variation between measurements within each sample were substantial, which could be a result of the uneven exposure of CuO on the catalyst surface.

In vitro testing of NO generation by CuO/SiO_2 nanocatalysts

It is known that cleavage of the S–NO bond in *S*-nitrosothiols to release NO occurs by an oxidation–reduction mechanism.[53–55] Copper ion-mediated catalytic decomposition requires Cu^{2+} to be first reduced to Cu^{1+} (Scheme 3). Under physiological conditions reducing agents for conversion of Cu^{2+} to Cu^{1+} can be the endogenous thiols, such as glutathione (GSH), which is present in blood in sufficient concentration. Copper(I) reacts with *S*-nitrosothiols, such as *S*-nitrosoglutathione (GSNO) to liberate NO by transferring an electron, and thus forms a thiolate anion, which is immediately protonated as a base to form a thiol, and regenerates Cu^{2+} (Scheme 3).

Several reports showed that such redox reactions can occur on surfaces containing immobilized complexes of Cu.[20–23,27,28] Metallic copper(0) nanoparticles of 80 nm were also used to create NO-generating polymer coatings, however their catalytic action was found to be due to the leaching of Cu^{2+} ions into solution caused by corrosion of the material.[34] Metallic copper-doped TiO_2 films were also shown to induce NO generation from an endogenous NO donor (though in those materials copper was mainly found to be in Cu^{2+} state).[35] So far, copper(II) oxide nanoparticles have not been directly studied for such catalytic activity.

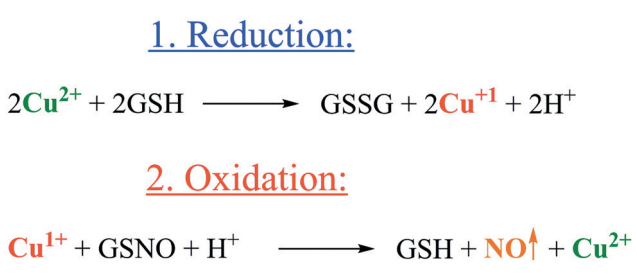

Scheme 3 Cu^{2+}/Cu^{1+} mediated NO generation.

In our work the catalytic effect of CuO/SiO_2 nanoparticles on NO generation was measured over a range of GSNO concentrations (0.01–1 mM). It was found that while unmodified silica did not influence the level of GSNO decomposition, 1 mg of nanocatalyst CuO/SiO_2_1 generated NO over 30 min incubation at all concentrations of GSNO substrate in the studied range, with a maximum concentration of NO detected from the decomposition of 1 mM GSNO (Fig. 6). The catalytic activity measured at 0.01 mM GSNO indicates that the nanocatalyst CuO/SiO_2_1 may well be active at substrate concentrations near the reported human plasma *S*-nitrosothiols level of 7 μM.[18]

Catalytic NO generation as a function of incubation time

The kinetics of NO release from GSNO catalyzed by CuO nanoparticles was investigated for the period of up to-90 min. Maximal NO release was reached after 30 min of catalyst incubation with 0.1 mM GSNO, after which its rate slowed down due to the gradual depletion of the substrate concentration in batch experiments (Fig. 7).

Catalytic NO generation as a function of CuO content and nanoparticle mass

All four CuO/SiO_2_1–4 samples were investigated to determine the relationship between the amount of CuO in the CuO/SiO_2 preparations and their catalytic activity. The direct comparison of equal quantities of the nanocatalyst preparations (1 mg of each)

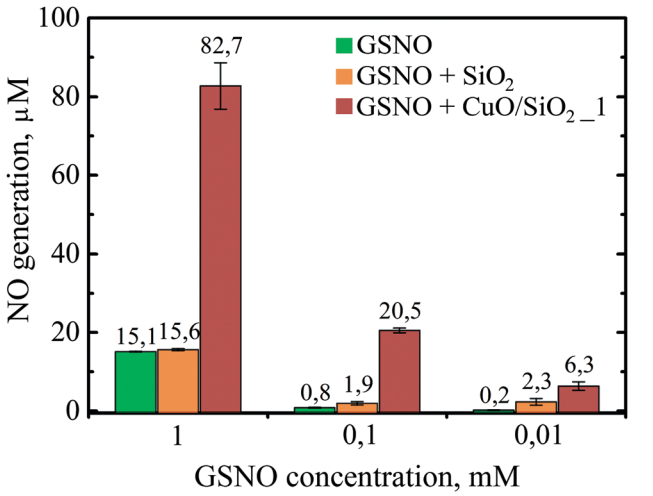

Fig. 6 Relationship between GSNO concentration and NO generation catalyzed by CuO nanoparticles. GSNO (1 mM, 0.1 mM, and 0.01 mM in 0.5 mL PBS) was incubated for 30 min, at 37 °C with 1 mg of CuO/SiO_2 *vs.* SiO_2 and nitrite generated was measured using the Griess assay. Values are mean of 3 measurements ± SD.

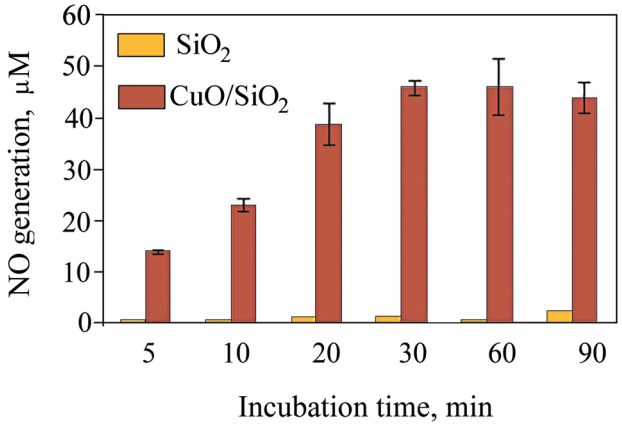

Fig. 7 CuO nanoparticle-catalysed NO release as a function of time. GSNO (0.1 mM in PBS) was incubated for 5–90 min at the presence of 1 mg of CuO/SiO_2 *vs.* SiO_2 and nitrite generation was measured using a Griess assay.

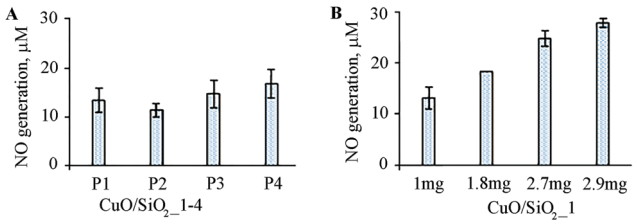

Fig. 8 Catalytic NO generation by four CuO/SiO_2_1–4 preparations measured with Griess assay: (A) 1 mg of each preparation was incubated with 0.1 mM GSNO in PBS for 30 min. (B) The amounts of CuO/SiO_2_1 matched the CuO content in 1 mg CuO/SiO_2_2 (1.8 mg), CuO/SiO_2_3 (2.7 mg) and CuO/SiO_2_4 (2.9 mg) incubated with 0.1 mM in PBS GSNO after 30 min.

showed no significant difference in the rate of NO generation between them after 30 min incubation (Fig. 8A).

Comparison of CuO/SiO_2_1 amount with matching CuO content to preparations 2–4 (the copper(II) oxide range in the CuO/SiO_2_1 preparation was between 0.026 mg and 0.075 mg) showed a tendency for increasing the amount of NO release by a higher amount of CuO (Fig. 8B).

This may indicate that the catalytic activity of nanoscale CuO/SiO_2_1–4 compositions depends to a certain extent on both the CuO amount in the sample and the degree of its exposure on the nanoparticle surface. Similar behavior of gold particles was described by Taladriz-Blanco *et al.*[56] who showed an increase in NO generation with a larger number of available active sites on the surface.

Our results show that NO generation can be catalyzed by nanosized CuO/SiO_2_1–4 compositions. It could be suggested that the oxidation–reduction mechanism involving Cu(II)–Cu(I) conversion (as depicted in Scheme 3) occurs on the surface of CuO/SiO_2 nanoparticles similar to homogeneous catalytic reactions involving copper ions in solution.

The stoichiometry of the surface of transition metal oxides often deviates from their typical bulk state lattice arrangement due to structural and electronic defects and they may contain species in different oxidation states on the surface. This phenomenon is particularly noticeable for nanoparticles with high surface-to-volume ratio.[57] For example, Cu^{2+} ions are known to be present on the surface of Cu_2O nanoparticles, CeO_2 nanoparticles are known to contain ions of Ce^{3+}, *etc.*[58–60] The existence of such defects in the oxide lattice influences the redox properties and the coordination environment of surface atoms, which are the key factors determining the catalytic properties of metal oxides.[58] Surface defects in many cases favour the transport of oxygen and thus may facilitate the conversion between Cu^{2+} and Cu^{1+} oxidation states. A facile exchange between oxidized and reduced states is essential for the GSNO decomposition reaction and could be the origin of the observed catalytic activity of CuO/SiO_2 compositions. The fact that, according to the XRD data, only CuO crystalline phase was present in the catalyst preparations CuO/SiO_2_1–4 may be due to its low sensitivity as a surface analytical technique and/or to the absence of bulk phase transitions.

Assessment of catalytic NO generation by CuO/SiO_2 in bovine serum using an ion-selective micro-electrode method

To determine the catalytic activity of the CuO/SiO_2 compositions in a physiological environment, the measurement of NO generation in bovine blood serum was performed. As an alternative to the Griess method for NO valuation, nitrite and nitrate ion-selective microelectrodes were used for an independent measurement of these ions in PBS and in bovine serum. Measurements of both nitrite and nitrate ions under the same conditions showed that CuO/SiO_2_2 produced significantly more NO in both PBS and bovine serum than in controls (Fig. 9). In bovine serum the catalytic activity was lower than in PBS by 23% ($p < 0.05$) (Fig. 9).

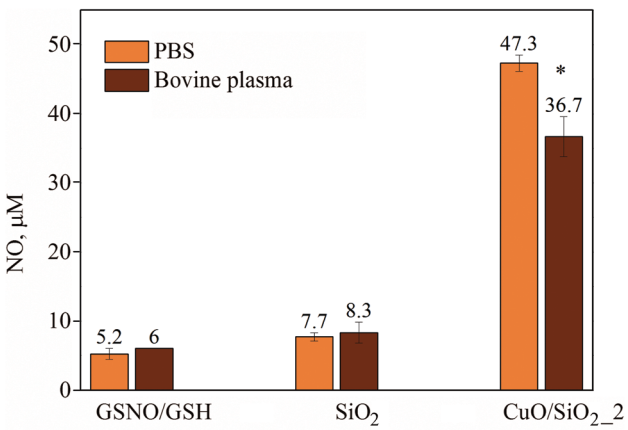

Fig. 9 Catalytic NO generation by CuO/SiO_2_2 in phosphate buffer saline, PBS and bovine serum. Experimental conditions: incubation of 1 mL of the solution of 100 μM GSNO and 100 μM GSH for 1 h at 37 °C in the presence of 1 mg of the catalyst. Controls: (i) GSNO/GSH: without addition of a solid oxide; and (ii) SiO_2: in the presence of 1 mg of SiO_2. Nitrite and nitrate concentrations were measured using ion-selective electrodes and combined to give the NO concentration values shown. Values are mean of 3 measurements ± SD. *$p < 0.05$.

The ability of CuO/SiO_2 to generate NO from endogenous NO-bearing substances opens a new route to designing novel medical polymers with immobilized CuO/SiO_2 NPs. Such polymers will be able to generate NO in contact with blood thus significantly improving their haemocompatibility and performance. The use of CuO/SiO_2 nanomaterials would be advantageous in comparison with other copper-containing compounds such as Cu MOFs, which require cumbersome synthesis and catalytic activity of which depends on the hydrophilicity of the polymer matrix.[29,61,62]

Conclusions

Novel CuO/SiO_2 compositions with CuO particle size in the range of 71–88 nm were synthesized. The ability of the synthesized nanomaterials to catalyze NO generation from *S*-nitrosoglutathione, an endogenous component of blood, was demonstrated. The generation of NO by CuO/SiO_2 catalyst from GSNO substrate was effective in physiological media such as phosphate buffered saline and bovine serum. The catalytic activity of CuO/SiO_2 compositions was found to depend on both the content of CuO in the sample and the accessibility of CuO nanoparticles on the material surface. The advantage of CuO/SiO_2 nanocomposites over other copper catalysts for RSNO decomposition is due to their unique features such as a high surface area, uniform dispersion and stability of the active catalytic species, and controllable particle size which allows fine tuning of their structure and properties. CuO/SiO_2 NPs can be incorporated into different polymer matrices used in biomedical applications such as surgical tubing, peripheral venous catheters, auxiliary blood circulation devices and drug-eluting balloons. Polymers with NO generating properties at blood-biomaterial interface thus obtained are expected to have improved biocompatibility which enhances their potential for use in biomedicine.

Conflicts of interest

There are no conflicts to declare.

Acknowledgements

The research was supported by the European Union's Seventh Framework Programme IRSES grant NANOBIOMAT (PIRSES-GA-2013-6124484). Liana Azizova acknowledges financial support of the Horizon 2020 project DualFun (H2020-MSCA-IF-2016, grant agreement No. 749207) as Marie Skłodowska-Curie Fellow.

Notes and references

1 B. D. Ratner, A. S. Hoffman, F. J. Schoen and J. E. Lemons, *Biomaterials Science: An Introduction to Materials in Medicine*, Academic Press, Oxford, UK, 3rd edn, 2013.
2 Biomaterials Market by Type of Materials (Metallic, Ceramic, Polymers, Natural) & by Application (Cardiovascular, Orthopedic, Dental, Plastic Surgery, Wound Healing, Neurological disorders, Tissue Engineering, Ophthalmology) - Global Forecast to 2024. Market Research Report (2019). MarketsandMarkets™ Inc. Northbrook, IL, USA, 2019.
3 World Population Prospects 2019: Highlights (ST/ESA/SER.A/423). United Nations, Department of Economic and Social Affairs, Population Division, 2019.
4 A. De Mel, F. Murad and A. M. Seifalian, Nitric oxide: A guardian for vascular grafts?, *Chem. Rev.*, 2011, **111**, 5742.
5 A. Dwyer, Surface-treated catheters - A review, *Seminars in Dialysis*, 2008, **21**, 542.
6 M. Joner, A. V. Finn, A. Farb, E. K. Mont, F. D. Kolodgie, E. Ladich, R. Kutys, K. Skorija, H. K. Gold and R. Virmani, Pathology of drug-eluting stents in humans: Delayed healing and late thrombotic risk, *J. Am. Coll. Cardiol.*, 2006, **48**, 193.
7 F. Jung, S. Braune and A. Lendlein, Haemocompatibility testing of biomaterials using human platelets, *Clin. Hemorheol. Microcirc.*, 2013, **53**, 97.
8 T. F. Lüscher, J. Steffel, F. R. Eberli, M. Joner, G. Nakazawa, F. C. Tanner and R. Virmani, Drug-eluting stent and coronary thrombosis, *Circulation*, 2007, **115**, 1051.
9 B. D. Ratner, The catastrophe revisited: Blood compatibility in the 21st Century, *Biomaterials*, 2007, **28**, 5144.
10 D. Tousoulis, A. M. Kampoli, C. Tentolouris, N. Papageorgiou and C. Stefanadis, The role of nitric oxide on endothelial function, *Curr. Vasc. Pharmacol.*, 2012, **10**, 4.
11 Z. M. Ruggeri, Platelets in atherothrombosis, *Nat. Med.*, 2002, **8**, 1227.
12 A. W. Carpenter and M. H. Schoenfisch, Nitric oxide release: Part II. Therapeutic applications, *Chem. Soc. Rev.*, 2012, **41**, 3742.
13 P. N. Coneski and M. H. Schoenfisch, Nitric oxide release: Part III. Measurement and reporting, *Chem. Soc. Rev.*, 2012, **41**, 3753.
14 M. C. Frost, M. M. Reynolds and M. E. Meyerhoff, Polymers incorporating nitric oxide releasing/generating substances for improved biocompatibility of blood-contacting medical devices, *Biomaterials*, 2005, **26**, 1685.
15 N. Naghavi, A. De Mel, O. S. Alavijeh, B. G. Cousins and A. M. Seifalian, Nitric oxide donors for cardiovascular implant applications, *Small*, 2013, **9**, 22.
16 D. A. Riccio and M. H. Schoenfisch, Nitric oxide release: Part I. Macromolecular scaffolds, *Chem. Soc. Rev.*, 2012, **41**, 3731.
17 A. B. Seabra and N. Durán, Nitric oxide-releasing vehicles for biomedical applications, *J. Mater. Chem.*, 2010, **20**, 1624.
18 J. S. Stamler, O. Jaraki, J. Osborne, D. I. Simon, J. Keaney, J. Vita, D. Singel, C. R. Valeri and J. Loscalzo, Nitric oxide circulates in mammalian plasma primarily as an *S*-nitroso adduct of serum albumin, *Proc. Natl. Acad. Sci. U. S. A.*, 1992, **89**, 7674.
19 Y. Wu and M. E. Meyerhoff, Nitric oxide-releasing/generating polymers for the development of implantable chemical sensors with enhanced biocompatibility, *Talanta*, 2008, **75**, 642.
20 S. Hwang, W. Cha and M. E. Meyerhoff, Polymethacrylates with a covalently linked Cu II –cyclen complex for the in situ generation of nitric oxide from nitrosothiols in blood, *Angew. Chem., Int. Ed.*, 2006, **45**, 2745.

21 K. Liu and M. E. Meyerhoff, Preparation and characterization of an improved Cu^{2+}–cyclen polyurethane material that catalyzes generation of nitric oxide from S-nitrosothiols, *J. Mater. Chem.*, 2012, **22**, 18784.
22 B. K. Oh and M. E. Meyerhoff, Spontaneous catalytic generation of nitric oxide from *S*-nitrosothiols at the surface of polymer films doped with lipophilic copper(II) complex, *J. Am. Chem. Soc.*, 2003, **125**, 9552.
23 B. K. Oh and M. E. Meyerhoff, Catalytic generation of nitric oxide from nitrite at the interface of polymeric films doped with lipophilic Cu(II)-complex: a potential route to the preparation of thromboresistant coatings, *Biomaterials*, 2004, **25**, 283.
24 Z. Yang, Y. Yang, K. Xiong, J. Wang, H. Lee and N. Huang, Metal-phenolic surfaces for generating therapeutic nitric oxide gas, *Chem. Mater.*, 2018, **30**, 5220.
25 F. Zhang, Q. Zhang, X. Li, N. Huang, X. Zhao and Z. Young, Mussel-inspired dopamine-Cu(II) coatings for sustained in situ generation of nitric oxide for prevention of stent thrombosis and restenosis, *Biomaterials*, 2019, **194**, 117.
26 V. Wonoputri, C. Gunawan, S. Liu, N. Barraud, L. H. Yee, M. Lim and R. Amal, Copper complex in poly(vinyl chloride) as a nitric oxide-generating catalyst for the control of nitrifying bacterial biofilms, *ACS Appl. Mater. Interfaces*, 2015, **7**, 22148.
27 S. Hwang and M. E. Meyerhoff, Polyurethane with tethered copper(II)–cyclen complex: Preparation, characterization and catalytic generation of nitric oxide from S-nitrosothiols, *Biomaterials*, 2008, **29**, 2443.
28 S. C. Puiu, Z. Zhou, C. C. White, L. J. Neubauer, Z. Zhang, L. E. Lange, J. A. Mansfield, M. E. Meyerhoff and M. M. Reynolds, Metal ion-mediated nitric oxide generation from polyurethanes via covalently linked copper(II)-cyclen moieties, *J. Biomed. Mater. Res., Part B*, 2009, **91**, 203.
29 J. L. Harding, J. M. Metz and M. M. Reynolds, A tunable, stable, and bioactive MOF catalyst for generating a localized therapeutic from endogenous sources, *Adv. Funct. Mater.*, 2014, **24**, 7503.
30 J. L. Harding and M. M. Reynolds, Metal organic frameworks as nitric oxide catalysts, *J. Am. Chem. Soc.*, 2012, **134**, 3330.
31 J. L. Harding and M. M. Reynolds, Composite materials with embedded metal organic framework catalysts for nitric oxide release from bioavailable S-nitrosothiols, *J. Mater. Chem. B*, 2014, **2**, 2530.
32 M. J. Neufeld, J. L. Harding and M. M. Reynolds, Immobilization of metal–organic framework copper(II) benzene-1,3,5-tricarboxylate (CuBTC) onto cotton fabric as a nitric oxide release catalyst, *ACS Appl. Mater. Interfaces*, 2015, **7**, 26742.
33 L. Azizova, S. Ray, S. Mikhalovsky and L. Mikhalovska, Development of Cu-modified PVC and PU for catalytic generation of nitric oxide, *Colloids Interfaces*, 2019, **3**, 33.
34 T. C. Major, D. O. Brant, C. P. Burney, K. A. Amoako, G. M. Annich, M. E. Meyerhoff, H. Handa and R. H. Bartlett, The hemocompatibility of a nitric oxide generating polymer that catalyzes *S*-nitrosothiol decomposition in an extracorporeal circulation model, *Biomaterials*, 2011, **32**, 5957.
35 Y. Xu, J.-A. Li, L.-F. Yao, L.-H. Li, P. Yang and N. Huang, Preparation and characterization of Cu-doped TiO_2 thin films and effects on platelet adhesion, *Surf. Coat. Technol.*, 2015, **261**, 436.
36 J. Pant, M. J. Goudie, S. P. Hopkins, E. J. Brisbois and H. Handa, Tunable nitric oxide release from S-nitroso-N-acetylpenicillamine via catalytic copper nanoparticles for biomedical applications, *ACS Appl. Mater. Interfaces*, 2017, **9**, 15254.
37 A. T. Bell, The impact of nanoscience on heterogeneous catalysis, *Science*, 2003, **299**, 1688.
38 J. A. Dahl, B. L. S. Maddux and J. E. Hutchison, Toward greener nanosynthesis, *Chem. Rev.*, 2007, **107**, 2228.
39 M. C. Frost and M. E. Meyerhoff, Controlled photoinitiated release of nitric oxide from polymer films containing *S*-nitroso-*N*-acetyl-DL-penicillamine derivatized fumed silica filler, *J. Am. Chem. Soc.*, 2004, **126**, 1348.
40 D. A. Riccio, J. L. Nugent and M. H. Schoenfisch, Stöber synthesis of nitric oxide-releasing S-nitrosothiol-modified silica particles, *Chem. Mater.*, 2011, **23**, 1727.
41 L. J. Ignarro, J. M. Fukuto, J. M. Griscavage, N. E. Rogers and R. E. Byrns, Oxidation of nitric oxide in aqueous solution to nitrite but not nitrate: comparison with enzymatically formed nitric oxide from L-arginine, *Proc. Natl. Acad. Sci. U. S. A.*, 1993, **90**, 8103.
42 K. M. Miranda, M. G. Espey and D. A. Wink, A rapid, simple spectrophotometric method for simultaneous detection of nitrate and nitrite, *Nitric oxide*, 2001, **5**, 62.
43 D. Giustarini, R. Rossi, A. Milzani and I. Dalle-Donne, Nitrite and nitrate measurement by Griess reagent in human plasma: Evaluation of interferences and standardization, in *Nitric Oxide, Part F. Methods in Enzymology*, ed. E. Cadenas and L. Packer, Academic Press - Elsevier, Cambridge, MA, USA, vol. 440, *ch. 23*, 2008, pp. 361–380.
44 E. M. Hetrick and M. H. Schoenfisch, Analytical chemistry of nitric oxide, *Annu. Rev. Anal. Chem.*, 2009, **2**, 409.
45 F. Michelet, R. Gueguen, P. Leroy, M. Wellman, A. Nicolas and G. Siest, Blood and plasma glutathione measured in healthy subjects by HPLC: relation to sex, aging, biological variables, and life habits, *Clin. Chem.*, 1995, **41**, 1509.
46 J. P. Richie, L. Skowronski, P. Abraham and Y. Leutzinger, Blood glutathione concentrations in a large-scale human study, *Clin. Chem.*, 1996, **42**, 64.
47 F. Tang, L. Li and D. Chen, Mesoporous silica nanoparticles: Synthesis, biocompatibility and drug delivery, *Adv. Mater.*, 2012, **24**, 1504.
48 V. Tertykh, Novel Aspects of the Chemical Modification of Silica Surface, in *Organosilicon Chemistry III: From Molecules to Materials*, ed. N. Auner and J. Weis, Wiley-VCH Verlag, Weiheim, Germany, 1998, ch. 104, pp. 670–681.
49 L. T. Zhuravlev, The surface chemistry of amorphous silica. Zhuravlev model, *Colloids Surf., A*, 2000, **173**, 1.
50 D. A. Thornton, Infrared spectra of metal β-ketoenolates and related complexes, *Coord. Chem. Rev.*, 1990, **104**, 173.
51 L. J. Bellamy, *The Infrared Spectra of Complex Molecules: Advances in Infrared Group Frequencies*, Chapman and Hall, London – New York, vol. 2, 1980.

52 K. Kulyk, M. Borysenko, T. Kulik, L. Mikhalovska, J. D. Alexander and B. Palianytsia, Chemisorption and thermally induced transformations of polydimethylsiloxane on the surface of nanoscale silica and ceria/silica, *Polym. Degrad. Stab.*, 2015, **120**, 203.

53 D. R. Noble, H. R. Swift and D. L. H. Williams, Nitric oxide release from *S*-nitrosoglutathione (GSNO), *Chem. Commun.*, 1999, 2317.

54 D. L. H. Williams, The chemistry of *S*-nitrosothiols, *Acc. Chem. Res.*, 1999, **32**, 869.

55 J. Lee, L. Chen, A. H. West and G. B. Richter-Addo, Interactions of organic nitroso compounds with metals, *Chem. Rev.*, 2002, **102**, 1019.

56 P. Taladriz-Blanco, V. Pastoriza-Santos, J. Pérez-Juste and P. Hervés, Controllable nitric oxide release in the presence of gold nanoparticles, *Langmuir*, 2013, **29**, 8061.

57 D. Neagu, G. Tsekouras, D. Miller, H. Ménardand and J. T. S. Irvine, *In situ* growth of nanoparticles through control of non-stoichiometry, *Nat. Chem.*, 2013, **5**, 916.

58 M. Fernández-García and J. A. Rodriguez, *Encyclopedia of Inorganic and Bioinorganic Chemistry*, John Wiley & Sons, 2009, ch. Metal oxide nanoparticles, p. 22.

59 K. Borgohain, N. Murase and S. Mahamuni, Synthesis and properties of Cu_2O quantum particles, *J. Appl. Phys.*, 2002, **92**, 1292.

60 S. Tsunekawa, T. Fukuda and A. Kasuya, Blue shift in ultraviolet absorption spectra of monodisperse CeO_{2-x} nanoparticles, *J. Appl. Phys.*, 2000, **87**, 1318.

61 M. J. Neufeld, A. Lutzke, W. M. Jones and M. M. Reynolds, Nitric oxide generation from endogenous substrates using metal-organic frameworks: inclusion within poly(vinyl alcohol) membranes to investigate reactivity and therapeutic potential, *ACS Appl. Mater. Interfaces*, 2017, **9**, 35628.

62 M. J. Neufeld, A. Lutzke, J. B. Tapia and M. M. Reynolds, Metal–organic framework/chitosan hybrid materials promote nitric oxide release from *S*-nitrosoglutathione in aqueous solution, *ACS Appl. Mater. Interfaces*, 2017, **9**, 5139.